# Optical properties of amorphous $Sb_2Se_3$:Sn films

Praveen Kumar[a], T.S. Sathiaraj[b] and R. Thangaraj[a]*

[a]*Department of Applied Physics, Guru Nanak Dev University, Amritsar-143005, India;*
[b]*Department of Physics, University of Botswana, Gaborone, Botswana*

(*Received 22 April 2009; final version received 18 November 2009*)

The measurements and analysis of optical transmission and far-infrared (IR) reflectivity spectra of thermally evaporated $Sb_2Se_3$:Sn films are reported. The refractive index and film thickness have been determined from the upper and lower envelopes of the transmission spectra (Swanepoel's standard envelope method), measured at normal incidence, in the spectral range from 800 to 2500 nm. Values of the refractive index fit well to Cauchy's dispersion relation. The optical gap decreases with an increase in the Sn content, while a maximum in the tailing parameter and Urbach's energy occurs with only a small amount (~1 at %) of this additive. Characteristic vibrational bands for $SbSe_3$ structural units are revealed in the far-IR spectrum with no additional ones arising from the Sn additive. The Kramers–Kronig analysis has been used to calculate the dielectric constants and hence the longitudinal optic and transverse optic splitting for various compositions. The inclusion of Sn as a charged entity along with the Coulomb interactions which serve to polarize the glass medium is found to be responsible for these results.

**Keywords:** amorphous semiconductors; thin films; chalcogenide glasses; optical properties; refractive index; far-infrared reflectivity

## 1. Introduction

Different metallic elements have been added in small amounts to different chalcogenide alloys in order to improve the characteristics of the materials used in applications, such as phase-change random-access memories (PRAMs) [1–4]. The ternary $Ge_2Sb_2Te_5$ (GST) alloy is currently used as an active media in optical memories (CDs and DVDs) which exhibit the required reflectivity contrast between amorphous and the crystalline states [1]. The need for low-cost, high-speed and high-density non-volatile memories has paved the way for PRAMs and major efforts have been made on the incorporation of different additives in GST in order to improve the material characteristics suitable for this technology [2,3]. These additives influence the disordered structure of the network accompanied by changes in the electronic structure and hence, device characteristics. However, obstructions posed by lack of detailed knowledge of these systems and the inappropriateness of certain characterization techniques prevent us from completely understanding

these phenomena. All possible applications arise from their optical and electrical properties which are closely related to their structure and composition.

Fast crystallization has been observed for high Sb (>10 at %) content in the Sb–Se binary [5]. The optimization of the composition of Sb–Se alloy for lower power consumption with improved device reliability and operation speed has recently been investigated for PRAM applications [6]. The need to develop and understand the properties of new materials remains at the forefront for the scientific community. Incorporation of metallic additives Ag/Sn in GST changes the network/crystal structure leading to the improvement in properties, such as crystallization speed, crystallization and melting temperatures or thermal stability for low-current programming devices [2,3]. Sn additive to $Sb_2Se_3$ has been found to influence the electrical and photoconduction processes [4]. Spectral characterization along with physical properties are important to understand the role of additives in different binary or ternary systems and hence to the development of new materials having improved performance and reliability. The present work reports an analysis of the vibrational spectrum and its correlation with optical properties for the $Sb_2Se_3$:Sn system.

## 2. Experimental details

Thin films of bulk $(Sb_2Se_3)_{100-x}Sn_x$ $(0 \leq x \leq 7)$ samples were deposited in a high vacuum ($\sim 10^{-5}$ mbar) using a HINDHIVAC coating unit (Model no. 12A4D). Well-cleaned glass substrates held at room temperature and molybdenum boats containing the source material were used for the deposition [4]. After the deposition, the films were kept inside the vacuum chamber for 24 h to attain metastable equilibrium. The thickness of the films was measured with a surface profiler KLA Tencor P15. The amorphous nature of the samples was confirmed by the absence of diffraction peaks in X-ray diffraction. A Philips XL30 ESEM system with an EDAX attachment was used for studying the chemical composition of as-prepared films and found to be within ~1% error as compared to the bulk staring materials.

The transmittance $T$ of as-prepared films was measured with an UV–VIS–NIR spectrophotometer (VARIAN Cary 500) in the wavelength range 800–2500 nm. Infrared (IR) reflection spectra (50–700 $cm^{-1}$) of the thick films were obtained with an IFS 60 v/s vacuum Fourier transform interferometer (Bruker, Germany) equipped with reflectance attachment (11° off normal) having appropriate sources and detectors. All data were measured at room temperature with 2 $cm^{-1}$ resolution against high reflectivity aluminium mirror, and represent averages of 200 scans for each film sample. All the measurements were performed under vacuum $\sim 10^{-2}$ mbar. A least-squares curve fitting was used to estimate the errors in the present work.

## 3. Results

### 3.1. *Refractive index and absorption coefficient*

Figure 1 shows the transmission spectra (800–2500 nm) for the as-prepared films. Owing to the large difference in the value of the refractive index of the glass substrate ($n_s \sim 1.5$ in the spectral range of interest) and that of the thin $(Sb_2Se_3)_{100-x}Sn_x$ films,

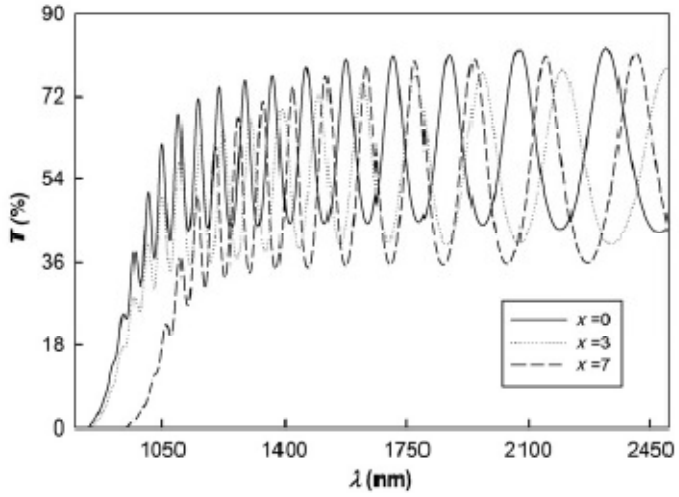


Figure 1. Transmission spectra for amorphous $(Sb_2Se_3)_{100-x}Sn_x$ films.

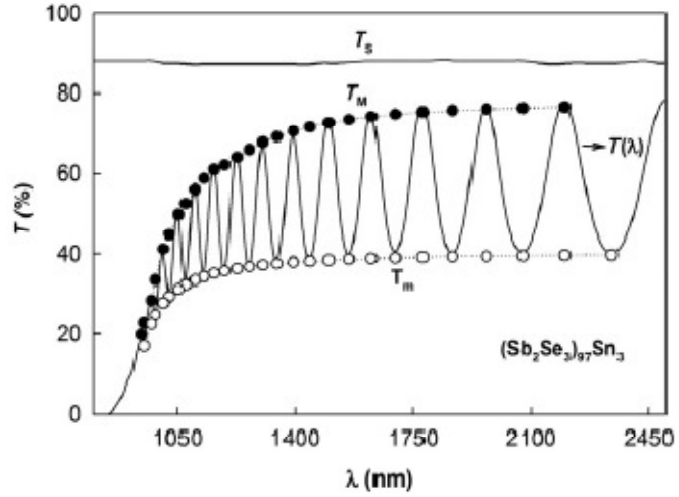


Figure 2. Typical transmission spectra for $(Sb_2Se_3)_{97}Sn_3$ films and the glass substrate ($T_S$). Curves $T_M$ and $T_m$ are the theoretically generated envelopes to the transmission spectrum.

extensive interference fringes appear in the transmission and reflection spectra. From the transmission spectrum (continuous lines), the values of $T_M$ and $T_m$ are the experimental interference extremes corresponding to maximum and minimum, respectively, and the other ones (dotted lines) are generated from a computer program. One such plot for $(Sb_2Se_3)_{97}Sn_3$ film is shown in Figure 2. Using Swanepoel's standard envelope method, the value of film thickness $t$ (found to be in good agreement with that measured by a surface profiler), refractive index $n$ and absorption coefficient $\alpha$ were determined, assuming the films have a homogeneous thickness and the glass substrate is completely transparent in the studied wavelength region [7–9]. The refractive index was found to decrease with increasing wavelength for all the films. The values of refractive index and extinction coefficient at 1.56 μm

are given in Table 1. The dispersion of refractive index has been studied using a model proposed by Cauchy [10,11]. It describes the normal dispersion of refractive index, namely the real part $n$ of the complex refractive index $N$ decreasing with increasing wavelength. This model is often used for dielectrics and semiconductors in the non-absorbing region (the imaginary part of $N$ is $k=0$). The Cauchy formula is as follows:

$$n(\lambda) = y_o + \frac{a}{\lambda^2} + \frac{b}{\lambda^4},$$

where $n$ represents the refractive index and $y_o$ describes the long-wavelength asymptotic value of the refractive index. The coefficients $a$ and $b$ add an upward slope to the index curve as the wavelength becomes shorter (both $a$ and $b \geq 0$, normal dispersion), i.e. $a$ controls the curvature of the middle part of the spectrum, while $b$ influences the spectrum at shorter wavelengths. All the glassy films studied were best fitted by the Cauchy model in the (900–2400 nm) spectral region (Figure 3). Table 1 summarizes the value of constants $y_o$ and $a$ for the present system. A positive value

Table 1. Value of thickness ($t$), Cauchy's dispersion parameters ($y_o$ and $a$), refractive index ($n$) and extinction coefficient ($k$) at 1.56 μm, optical gap ($E_o$), tailing parameter ($B^{-1}$) and Urbach's energy ($E_u$) for amorphous $(Sb_2Se_3)_{100-x}Sn_x$ films.

| $x$ | $t$ (μm) | $y_o$ (±0.01) | $a$ | $n$ | $k$ ($\times 10^{-8}$) | $E_o$ (±0.01 eV) | $B^{-1}$ (meV/cm) | $E_U$ (meV) |
|---|---|---|---|---|---|---|---|---|
| 0 | 2.69 | 2.95 | 616698.9 | 3.22 | 3.56 | 1.42 | 0.383 | 192.8 |
| 1 | 1.93 | 1.90 | 662632.0 | 2.20 | 1.12 | 1.36 | 1.154 | 608.3 |
| 3 | 2.43 | 2.76 | 631120.2 | 3.04 | 1.92 | 1.35 | 0.829 | 518.2 |
| 5 | 2.18 | 3.11 | 523297.9 | 3.64 | 2.38 | 1.31 | 0.501 | 360.1 |
| 7 | 2.86 | 3.33 | 350152.4 | 3.46 | 2.76 | 1.23 | 0.402 | 289.7 |

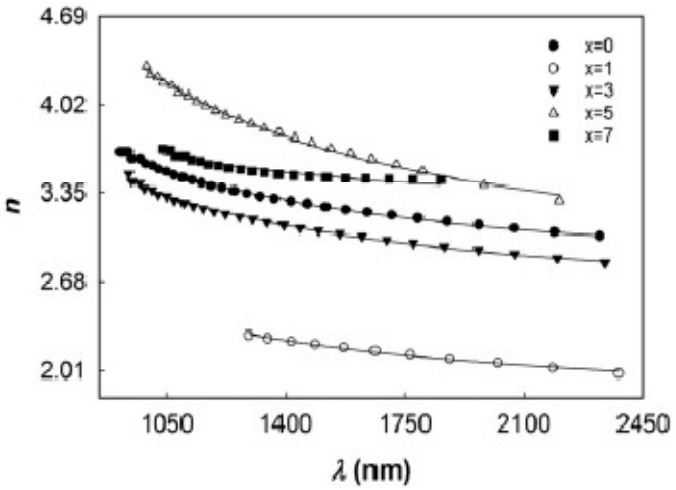


Figure 3. Spectral dependence of refractive index for $(Sb_2Se_3)_{100-x}Sn_x$ film samples. The solid line shows the Cauchy theoretical fit to the observed values.

of constant $b$ has been observed, indicating normal dispersion of the refractive index. All three parameters were used for the extrapolation of $n$ over the whole spectral range [10,12]. The values of $y_o$ and $a$ have opposite trends with increase in the Sn content.

Knowing the values of refractive index $n$ and film thickness $t$, the absorption coefficient can be calculated using the following relation: $\alpha = (1/t) \ln (y^{-1})$, where $y$ is the absorbance calculated from the interference extrema and/or the outer envelope function as proposed by Swanepoel et al. [7,8]. Figure 4 gives the spectral variation of absorption coefficient so obtained for $(Sb_2Se_3)_{100-x}Sn_x$ $(0 \leq x \leq 7)$ films. The value of the extinction coefficient $k$ can be calculated using the relation $\alpha = \lambda/4\pi k$ and its value is summarized for all compositions at 1.56 μm in Table 1. Near the fundamental absorption region ($10^4$–$10^5\,cm^{-1}$), the absorption coefficient is given by $\alpha h\nu = B(h\nu - E_o)^2$, where $E_o$ is the optical gap and $B^{1/2}$ is the slope in the extended region and is a measure of the extent of band tailing for a given material. Figure 5 shows the plots of $(\alpha h\nu)^{1/2}$ versus photon energy $(h\nu)$ from which the values of optical gap $E_o$ and the slope or tailing parameter $B^{-1}$ are determined for all the samples. Table 1 summarizes both these parameters for the present system. Its value for $x = 0$ is found to be in good agreement with the theoretically calculated one using the Shimakawa relation for the random network [13]. The value of the optical gap decreases linearly with composition, while a large value of the tailing parameter $B^{-1}$ for $x = 1$ has been observed. The spectral region with absorption coefficient $(10^2 < \alpha < 10^4\,cm^{-1})$ is called the Urbach exponential tail region, where the absorption coefficient is given by $\alpha = \alpha_o \exp(h\nu/E_U)$, where $E_U = d(h\nu)/d(\ln \alpha)$ is the Urbach energy. Most optical transitions take place between localized tail states and extended band states [14]. The inset of Figure 5 shows one such plot for $(Sb_2Se_3)_{99}Sn_1$ films, where a plot of $\ln \alpha$ versus $h\nu$ yields a straight line revealing that the absorption tail corresponds to an exponential edge. Its large value for $x = 1$ shows an enhancement in the randomness of the network structure with a decrease in the optical gap.

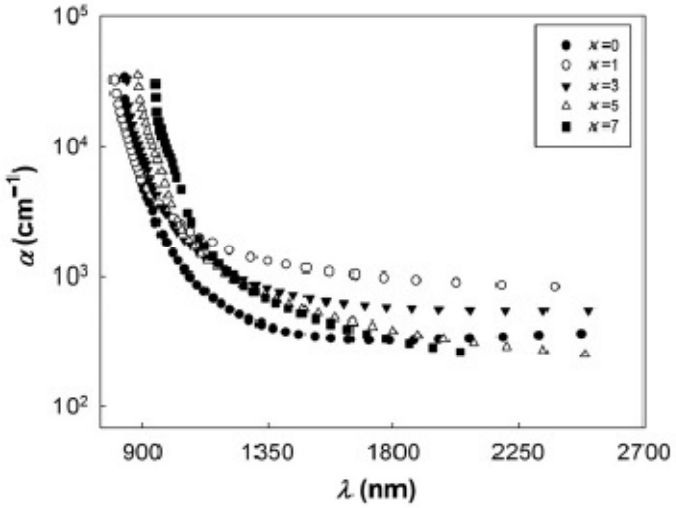


Figure 4. Variation of absorption coefficient with energy for $(Sb_2Se_3)_{100-x}Sn_x$ films.

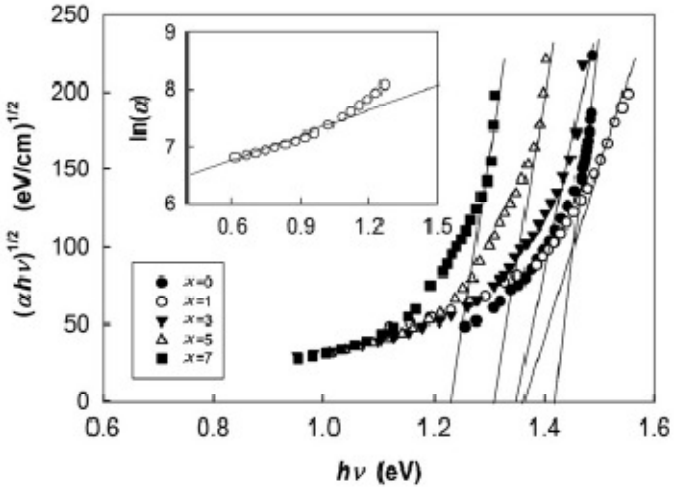


Figure 5. Plot of $(\alpha h\nu)^{1/2}$ versus $h\nu$ for $(Sb_2Se_3)_{100-x}Sn_x$ film samples. The inset picture shows the variation of $\ln\alpha$ with $h\nu$ for the $(Sb_2Se_3)_{99}Sn_1$ film.

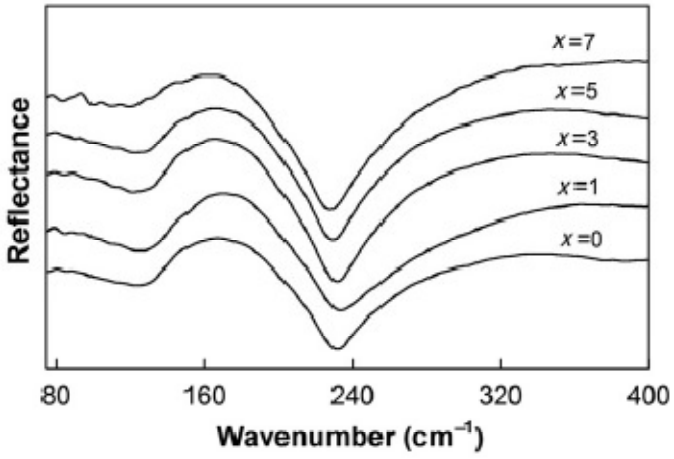


Figure 6. Composition dependence of far-IR reflectivity spectrum for amorphous $(Sb_2Se_3)_{100-x}Sn_x$ films.

### 3.2. *Vibrational spectrum*

Information on structural features to help understanding the optical properties was obtained using far-IR reflectivity spectra. Figure 6 shows spectrum for the amorphous $(Sb_2Se_3)_{100-x}Sn_x$ $(0 \leq x \leq 7)$ films. On account of the broad shape, the reflectivity bands were analyzed by de-convoluting those located in the 230–130 and 560–230 cm$^{-1}$ spectral regions. Main vibrational bands were observed at 287.3, 193.9 and 162.4 cm$^{-1}$. The spectral domain 50–110 cm$^{-1}$ is characterized by weak bands for $Se_n$ chains (90 cm$^{-1}$), $Sb(Se_{1/2})_3$ pyramids (78 cm$^{-1}$) and bending modes of $Sn(Se_{1/2})_4$ tetrahedra (102–123 cm$^{-1}$), respectively.

Strong nearest-neighbor forces serve as mechanical constraints in stabilizing a glass network [15], while weak Coulomb forces promote only space filling of the

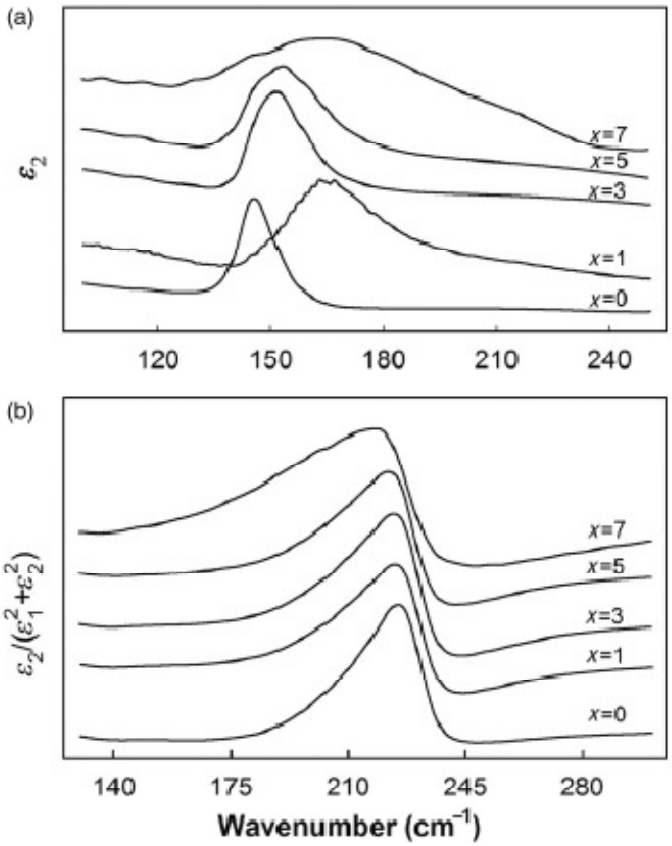


Figure 7. Spectral dependence of $\varepsilon_2$ and $\varepsilon_2/(\varepsilon_1^2+\varepsilon_2^2)$ with wavenumber for $(Sb_2Se_3)_{100-x}Sn_x$ films.

network glasses. The Coulomb interactions also serve to polarize a glass medium and as a consequence one observes splitting between the longitudinal optic (LO) and transverse optic (TO) vibrational modes, respectively [16–19]. The TO mode is mainly associated with vibrations parallel to the sample surface, while the LO mode is related to vibrations perpendicular to the surface [18]. It is therefore interesting to study the TO/LO splitting, the difference of which provides information about the extent of polarization of the network. Kramers–Kronig (K–K) transformations constitute one of the principal tools for the assessment of optical properties from measured spectra. From the far-IR reflectivity spectra of the films, the values of $n$ and $k$ can be derived by K–K transformations [16,17]. The real $\varepsilon_1$ and imaginary $\varepsilon_2$ parts of the complex dielectric constant have been computed and peaks in $\varepsilon_2$ and in $\varepsilon_2/(\varepsilon_1^2+\varepsilon_2^2)$ correspond, respectively, to the TO and LO split frequencies. Figure 7 shows such a plot for all the samples.

## 4. Discussion

The decrease in $E_o$ with Sn content can be correlated with the character of the chemical order of chalcogenide amorphous semiconductors. According to this model [20], the dominant contribution for states near the valence band edge comes from

their lone-pair p-orbital in materials having a large component of chalcogen atoms. The lone-pair electrons in these atoms adjacent to electropositive atoms will have higher energies than those close to the electronegative atoms. Therefore, the addition of electropositive elements to the alloy may raise the energy of some lone-pair states sufficiently to broaden the band inside the forbidden gap. This will give an initial steep increase in the value of the tailing parameter ($x = 1$). Even though the absorption edge shifts to higher energies, this gives a lower value of the gap, owing to the differences in the electro-negativities (Sn, Sb and Se are 1.8, 1.9 and 2.4, respectively), Sn goes into the network as a charged entity and raises the energy of the chalcogen lone-pair states, broadening the valence band [4] and thus giving a large value of the tailing parameter or Urbach energy with a decrease in the optical gap. This will give rise to additional absorption over a wider range of energies leading to band tailing and hence a shrinking of the optical gap. A similar effect in the optical gap has also been observed with the Sn substitution for Ge in the amorphous Ge–Se system [21]. A higher concentration of the additive may lead to an increase in the number of wrong/heteropolar bonds in the network and further decrease the optical gap. These results suggest a change in the intermediate range ordering, which determines the majority of electronic and optical phenomena in this semiconducting system.

The observation of vibrational bands for network building units in the far-IR spectrum gives information of local structural changes occurring on introduction of an additive to the parent alloy. Corredor et al. [22] have calculated the vibrational bands for $SbSe_3$ pyramidal units as 112, 315, 215 and 78 $cm^{-1}$ in Sb–As–Se glasses. Similarly, Smith et al. [23,24] have reported Raman-mode frequencies of 107.9 and 187.0 $cm^{-1}$ and IR active mode frequencies as 145.6 and 239.8 $cm^{-1}$ for $SnSe_2$ crystals. Therefore, characteristic peaks observed in the present work can be ascribed to stretching modes of Sb-pyramidal units (172–192 $cm^{-1}$) [22] and homopolar Sb–Sb bonds (170 $cm^{-1}$) [25] for our $Sb_2Se_3$ films. The contribution to the latter band cannot be distinguished; however, wrong bonds play a part in constituting the network of thermally evaporated films. The fact that these bands are not located as theoretically predicted could be due to the higher structural disorder present in the film structure. The band around 162.4 $cm^{-1}$ for $x = 0$ increases slightly to higher values for $x = 1$ to 166.2 $cm^{-1}$ and then decreases with a gradual drop in the intensity or amplitude. A similar trend has been observed for the 193.9 $cm^{-1}$ band. The full width at half maximum (FWHM) for all three bands were found to be maximum for $x = 1$, indicating a large influence on the structure of this binary system at low additive contents. Addition of Sn does not yield any new reflectivity bands in the spectrum, while it leads to a change in the position or widths of the various bands. Small addition results in a large shift in the band towards the higher wavenumber side (342.4 $cm^{-1}$) and thereafter, a shift to the lower wavenumber side with further addition. This can be ascribed to the different atomic masses and relative increase in the concentration of Sn–Se strong bonds, which affects the frequency of this band at higher wavenumbers. Formation of mixed structural units with the substitution of Sn in Sb-pyramidal units leads to distinct changes in the reflectivity and this is ascribed to the larger atomic weight of the metal additive. The gradual increase in metallic content is the cause for the anomalous trends in the observed results.

The peak LO mode frequency shifts to the red, while the TO mode shows anomalous behavior with increasing $x$. There is a steep increase in the TO mode frequency with a small addition of Sn ($x=1$), then a sharp decrease for $x=3$ and thereafter, a blue shift with a broadening of the peak. The jump at $x=1$ for the TO mode frequency reflects an increased transverse stiffness caused by cross linking (the parent alloy $Sb_2Se_3$ has a layer structure) with an absence of fluctuating longitudinal internal network stresses. However, higher amounts of metallic additive favor the alloy formation, which may lead to the anomalous trends in the TO mode frequencies. The small difference in the LO/TO mode splitting frequencies for $x=1$ indicates a lower polarization or a decrease in the number of defects as the metallic additive leads to chemical alloying, but with an increase in the band tailing as observed from the optical analysis.

## 5. Conclusions

Optical characterization of thermally evaporated amorphous $(Sb_2Se_3)_{100-x}Sn_x$ ($0 \leq x \leq 7$) films has been carried out using transmittance spectra (800–2500 nm) and far-IR reflectance spectra (70–400 $cm^{-1}$). Swanepoel's standard envelope method has been applied to determine the refractive index, absorption coefficient and average thickness of the films. Cauchy's dispersion model was used to model the refractive index over the whole spectral region. The optical gap was found to decrease linearly with Sn content, while large values of the tailing parameter ($B^{-1}$) and the Urbach energy ($E_U$) for $x=1$ has been obtained. Vibrational bands associated with $SbSe_3$ structural units were observed for the binary alloy, while no Sn-related peaks/bands were observed in the spectra. The K–K analysis in the far-IR region was used to evaluate the dielectric constants and splitting frequencies for different optical modes (LO/TO).

## Acknowledgements

The authors wish to thank Prof. V. Venkataraman (Co-ordinator) and Dr. R. Ganesan (Scientific Officer) at the DST-National Facility for Low Temperatures and High Magnetic Fields, Department of Physics, Indian Institute of Science, Bangalore for providing access to the FTIR facility. One of the authors (PK) is grateful for the financial assistance from the CSIR, New Delhi, India.

## References

[1] T. Ohta and S.R. Ovshinsky, *Phase-change optical storage media*, in *Photo-induced Metastability in Amorphous Semiconductors*, Chapter 18, A.V. Kolobov, ed., Wiley-VCH GMBH, Berlin, 2003, p.310.
[2] K. Song, S. Kim, J. Seo and H. Lee, J. Appl. Phys. 104 (2008) p.103516.
[3] M.L. Lee, K.T. Yong, C.L. Gan, L.H. Ting, S.B.M. Daud and L.P. Shi, J. Phys. D Appl. Phys. 41 (2008) p.215402.
[4] P. Kumar and R. Thangaraj, Phil. Mag. Lett. 89 (4) (2009) p.241.
[5] D. Tonchev and S.O. Kasap, J. Non-Cryst. Solid. 248 (1999) p.28.

[6] S. Yoon, N. Lee, S. Ryu, K. Choi, Y. Park, S. Lee, B. Yu, M. Kang, S. Choi and M. Wuttig, IEEE Electron Device Lett. 27 (6) (2006) p.445.
[7] R. Swanepoel, J. Phys. E 17 (1984) p.896.
[8] E.G. El-Metwally, M.O. Abou-Helal and I.S. Yahia, J. Ovonic Res. 4 (2) (2008) p.20.
[9] E.R. Shaaban, M.A. Kaid, El Sayed Moustafa and A. Adel, J. Phys. D Appl. Phys. 41 (2008) p.125301.
[10] H.G. Tompkins and W.A. McGahan, *Spectroscopic Ellipsometry and Reflectometry*, Wiley Interscience, New York, 1999.
[11] L. Cauchy, Bull. Sci. Math. 14 (1830) p.9.
[12] R. Capan, N.B. Chaure, A.K. Hassan and A.K. Ray, Semicond. Sci. Tech. 19 (2004) p.198.
[13] K. Shimakawa, J. Non-Cryst. Solid. 43 (2) (1981) p.229.
[14] S.R. Elliott, *Physics of Amorphous Materials*, 2nd ed., Longman, London, 1990.
[15] M. Kastner, D. Adler and H. Fritzsche, Phys. Rev. Lett. 37 (1976) p.1504.
[16] M.H. Ali and S.A. Fayek, Phys. Status Solidi (a) 147 (2) (1995) p.577.
[17] C. Corredor, I. Quiroga, J. Vazquez, J. Galdon, P. Villares and R. Jimenez-Garay, Mater. Lett. 42 (2000) p.229.
[18] A.J. Smith, P.E. Meek and W.Y. Liang, J. Phys. C Solid State Phys. 10 (1997) p.1321.
[19] J.Y. Harbec and S. Jandl, Phys. Rev. B 25 (10) (1982) p.6126.
[20] S.M. El-Sayed, Semicond. Sci. Tech. 18 (2003) p.337.
[21] J.C. Philips, J. Non-Cryst. Solid. 34 (1979) p.153.
[22] F.L. Galeener and G. Lucovsky, Phys. Rev. Lett. 37 (1976) p.1474.
[23] R.M. Almeida, Phys. Rev. B 45 (1992) p.161.
[24] C.Z. Tan and J. Arndt, J. Chem. Phys. 112 (2000) p.5970.
[25] T.B. Wang, Z.G. Liu and C.Z. Tan, J. Chem. Phys. 119 (11) (2003) p.505.